Beam Profile Monitoring at the Test Beam Line at CTF3

Maja Olvegård,* E. Adli,† W. Andreazza, E. Bravin, N. Chritin, A. Dabrowski, S. Döbert, M. Duraffourg, T. Lefèvre, and R. Lillestøl†

CERN, European Organization of Nuclear Research, 1211 Geneve 23, Switzerland

(Dated: December 16, 2011)

The CLIC Test Facility 3 has been built, by an international collaboration at CERN, to demonstrate the feasibility of the CLIC RF source and the two-beam acceleration scheme. In particular, the Test Beam Line (TBL), is a small-scale drive beam decelerator and studies the transport of a high current electron beam as it is being decelerated in several Power Extraction and Transfer Structures (PETS). With a maximum of 16 structures, the beam will be decelerated from 150 MeV to a minimum of 67 MeV, while its energy spread increases significantly. In order to monitor the energy transfer a segmented beam dump for time-resolved spectrometry has been designed and installed at the end of the TBL. The segmented dump provides single-shot spectra with a 1 % resolution on energy and a 5 ns temporal resolution. Complementary to this, a single-slit dump, which provides fast spectrometry based on a multi-shot dipole scan technique, is installed at the beginning of the line, thus providing a measurement for comparison. This paper presents the first beam measurements at TBL, with an estimation of the performance of the segmented beam dump.

I. INTRODUCTION

The CLIC study (Compact Linear Collider) aims at a 3 TeV e^+e^- collider [1], based on a two-beam acceleration concept: A high intensity drive beam, decelerated in Power Extraction and Transfer Structures (PETS) [2] generates the 12 GHz RF power needed to accelerate the main beam. In each CLIC decelerator the drive beam is decelerated from 2.4 GeV to 240 MeV. The feasibility of this scheme is being addressed at the CLIC Text Facility (CTF3) [3] at CERN. One of the main activities is the commissioning of the Test Beam Line (TBL). TBL is a small-scale CLIC decelerator which, when complete, will include 16 consecutive PETS for drive beam deceleration. The study focuses on having a constant power production while maintaining the drive beam stable, with a minimum of particle losses [4].

A. CTF3

CTF3, depicted in Fig. 1 consists of four main parts: a) An injector and a linear accelerator, based on a DC thermionic gun, a 1.5 GHz subharmonic bunching system, a 3 GHz bunching system and 18 3 GHz accelerating structures operated under full beam-loading [5] conditions; b) a delay loop and a combiner ring; c) a CLic EXperimental area, CLEX; and d) a PHoto Injector test facility, PHIN. CTF3 is normally operated at 1 Hz pulse repetition rate, with rates up to 50 Hz possible.

The nominal beam energy at the end of the linac is 150 MeV, with a bunch frequency of 1.5 GHz. Through a complex scheme of interleaving a 1200 ns bunch train from the linac is transformed into a 140 ns bunch train with 8 times the bunch repetition frequency and average current. This high frequency, high intensity beam is then transported to CLEX for deceleration experiments in TBL and for two-beam acceleration in the Two-Beam Test Stand [6].

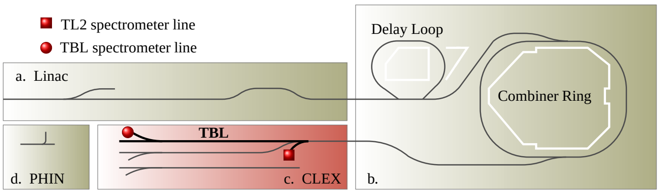

FIG. 1. A schematic layout of CTF3 showing the different parts and the spectrometer lines in connection to TBL.

CTF3 can be operated in various configurations. Beams bunched at either 1.5 GHz or 3.0 GHz can be produced by the injector. On top of this, the delay loop can be bypassed and the beam can be extracted from the combiner ring before the bunch recombination has been completed, thus delivering beams of different currents to CLEX.

B. The Test Beam Line

Similarly to the CLIC drive beam decelerator, the main part of the TBL [7] consists of a FODO lattice with a PETS in each drift space. There are 8 FODO cells, allowing for 16 PETS in total, of which 9 have been installed so far. Each quadrupole in the FODO lattice is mounted on a precision mover [8], allowing for efficient steering and beam-based alignment.

The PETS [9] is a passive microwave device, and consists of a periodically loaded waveguide, with a fundamental mode frequency of 12 GHz. Due to the high

* Also at Uppsala University, Department of Physics and Astronomy, Box 516, 751 20 Uppsala, Sweden; maja.olvegard@physics.uu.se; maja.olvegaard@cern.ch

† Also at University of Oslo, Boks 1072 Blindern, 0316 Oslo, Norway

impedance of the structure, the beam will leave a strong wakefield which builds up coherently with the high-intensity drive beam passing through. The field travels down the structure and is coupled out at the end, providing a high-power RF source to accelerate the main beam. Figure 2(a) shows a photograph of a PETS installed in TBL. The interior part of a PETS is presented in Fig. 2(b). At TBL the extracted power is only measured and not used for acceleration.

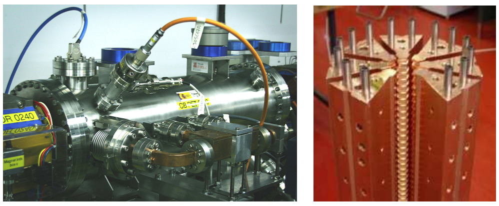

(a) A full PETS installed in TBL. (b) PETS structure

FIG. 2. Pictures of a TBL PETS.

In the CLIC design each PETS will produce 140 MW of power for the nominal beam current of 101 A. The power extracted from the beam will consequently lead to its deceleration. The deceleration scales linearly with the beam current. After each CLIC decelerator sector a total of 90 % of the beam power has been extracted, which leads to a growth of the transverse beam envelope and to a large energy spread at the end of the line. The CTF3 beam current is roughly a fourth of the CLIC beam current. In order to provide power of the same order of magnitude, the TBL PETS are four times longer than the PETS designed for CLIC. For a beam current of 28 A, at CTF3 each PETS will therefore produce approximately 140 MW of power and decelerate the beam by 5.2 MeV. With all PETS installed this means a deceleration from 150 MeV to 67 MeV, i.e. extraction of 55% of the beam energy. Due to the filling time of the PETS, there will be a 3 ns long high-energy transient followed by a long steady state, as depicted in Fig. 3. The energy distribution at the end of the line has been simulated in Placet [10, 11]. The large energy spread and the asymmetric energy distribution is clear in Fig. 4.

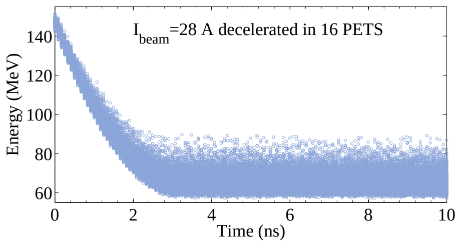

FIG. 3. A Placet simulation showing the beam energy distribution during the first 10 ns of a 28 A beam pulse, initially at 150 MeV, decelerated in 16 PETS. The 3 ns long high-energy transient is followed by a 137 ns steady state with an unusually large energy spread, see Fig. 4.

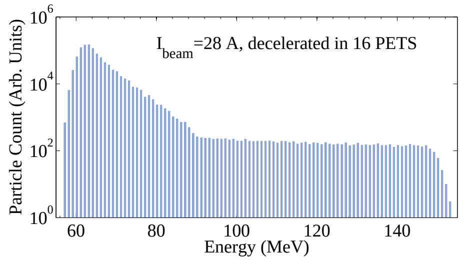

FIG. 4. Placet simulation: Histogram of the energy distribution of a 28 A beam decelerated in 16 PETS. The large energy spread is clearly visible, as well as the asymmetric profile, resulting from the high-energy transient.

C. Beam Profile Monitors at TBL

In designing interceptive beam diagnostic elements, a beam with an energy profile such as the one of the TBL beam, requires special attention. The unusually high intensity adds a first complexity to the project, in the aspect of heat-resistance and life time of equipment. At CTF3 a substantial effort has been put into the development of beam profile instruments adapted to high intensity beams and the demanding radiation environment. The beam instrumentation in TBL is built on developments done for the CTF3 linac, where the beam energy and energy spread is monitored in spectrometer lines [12].

The monitoring of the TBL beam is concentrated to two diagnostics sectors: one in TL2, just before TBL and one at the end of TBL, as marked in Fig. 1. Both sectors follow the same pattern and include an Optical Transition Radiation (OTR) screen for transverse profile measurements, another OTR screen for high resolution spectrometry, and a device for time-resolved spectrometry. Apart from these instruments TBL also holds inductive BPMs [13] for beam position and current monitoring, and a streak camera, imaging an OTR screen, for bunch length measurements.

The following two sections give a brief description of the OTR screen systems and a more detailed description of the time-resolved instruments.

II. OTR SCREENS FOR TRANSVERSE PROFILE

OTR screens play an important role in the CTF3 operation [14], so also for TBL. The screens for transverse profile measurements are employed mostly for determining the beam emittance and Twiss parameters through quadrupole scans. All OTR systems at CTF3 have a similar layout: A vacuum tank containing the OTR screens, an optical line from the view port of the tank to a CCD camera imaging the light emitted in the backward direction. The optical line generally includes an achromatic lens and optical density filters, as well as mirrors. The systems for transverse profile monitoring at TBL are depicted in Fig. 5(a) and are the latest implemented design. It comprises a few important new features:

- A four-positions system as shown in Fig. 5(b), where the first, starting from the right, consists of a replacement chamber. The replacement chamber was implemented to minimize the disturbance to the beam by diagnostic equipment when not in use.
- The second and the third positions hold the 30 mm screens, each 200 μm thick, polished to mirror quality. The first is made of CVD SiC, able to withstand the thermal load of the fully combined beam [15]. The second one, made of Si, though slightly worse from a thermal perspective, has a higher reflection coefficient and is therefore useful at lower current.
- The fourth position holds a calibration target, shown in Fig. 5(b), below. With the target, reference marks on the measurement screens are not needed and the calibration is easier.
- The tilt of the screen with respect to the beam has been reduced from the former standard of 45° to 15° in order to minimize field-depth aberrations.
- The length and complexity of the optical system have been significantly reduced. Merely two mirrors, one lens and optical density filters are placed between the screen and the CCD camera.
- The system has been made more compact by using a single girder containing the vacuum tank and the optical rail. In this way the overall alignment becomes more precise. Furthermore, a support for the camera with lead shielding ensures a long life time of the system by protecting the camera from radiation.

The emittance screens have a typical resolution of 50 μm, determined by the optical magnification and of the size of the CCD pixels.

The performance of the CTF3 screens have been thoroughly studied, refer to [14, 16, 17] for more details.

III. SPECTROMETRY

In spectrometry the beam energy is measured by determining the beam position in a dispersive region. The horizontal beam profile in the spectrometer, σ_x, is converted to a momentum profile, σ_p, through the following equation:

$$\frac{\sigma_p}{p_0} = \frac{1}{D}\sqrt{\sigma_x^2 - \varepsilon\beta} \tag{1}$$

where $D \approx L\theta$ is the dispersion function at the location of the spectrometer. The spectrometer angle θ corresponds to the reference particle momentum p_0. L is the length of the spectrometer arm, as measured from the center of the bend to the location of the detector. By subtracting $\sigma_0^2 = \varepsilon\beta$, from the measured beam size in quadrature the measurement is compensated for the intrinsic beam size, which is obtained through measurements of the Twiss parameters.

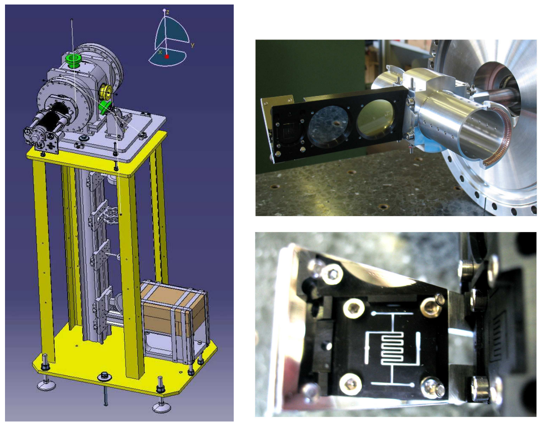

(a) OTR screen system (b) screen support with four positions (above), including a calibration target (below)

FIG. 5. OTR screen system for transverse beam profiling in TBL.

The spectrometer lines at TBL follow the general CTF3 standard for spectrometry [12, 18]. It comprises an OTR screen for high resolution energy and energy spread measurement in a single-shot, but with a 20 ms integration time. Behind the screen there is a device for time-resolved spectrometry for the monitoring of energy and energy spread along the pulse.

At CTF3 segmented beam dumps have been used for time resolved spectrometry [12]. These have shown to be simple, robust systems, well adapted to the high intensity beam at CTF3. A novel segmented beam dump was designed especially for the TBL. It was installed in January 2011 and commissioned during the Summer of 2011. In addition to this a single-slit dump is installed at the of the TL2 line, just before TBL, thus providing a reference measurement of the beam energy and energy spread before deceleration.

Table I contains information on the spectrometer lines in connection to TBL. The devices installed are shown, together with the relevant geometry information used in equation 1. The devices used in the spectrometer lines will be described below.

A. OTR for spectrometry

The OTR screen systems for spectrometry are slightly different from the transverse profile monitors. Instead of several screens and positions, there is only one fixed aluminum screen, 150 mm×50 mm surface area, 50 μm thick,

TABLE I. Characteristics of the spectrometer lines and its monitors used in the TBL study.

Location[a]	θ (°)	Device	L (mm)	Comment
TL2	22.5	OTR screen	1270	Parabolic[b]
TL2	22.5	Single-slit dump	2050	multi-shot
TBL	10	OTR screen	1260	Unpolished[b]
TBL	10	Segmented dump	2000	single-shot

[a] See CTF3 layout in Fig. 1.
[b] See section III A below

intercepting the beam path at a 45° angle. The backward OTR light is imaged with a CCD camera via a long line of lenses, mirrors and density filters, similarly to the other systems. In addition, there is a 50 μm carbon foil mounted in front of the screen. The foil is there to block synchrotron radiation generated in the dipole magnet. An example of such a screen support including a carbon foil is depicted in Fig. 6.

FIG. 6. A support for a 150 mm×50 mm surface area and 50 μm thick spectrometer screen with a carbon foil in front for blocking synchrotron radiation.

The OTR screen systems provide single-shot, high resolution spectrometry (better than 0.2% on energy spread). Since the standard integration time of the CCD cameras in use is 20 ms, the system lacks the temporal information that can be provided by the segmented dump. Nonetheless, it offers excellent opportunities for a comparison measurement, seeing that OTR is a well characterized technique for beam profiling [19]. It is also useful when the segmented dump falls short because of limited resolution.

The TBL spectrometer line holds a diffusive aluminum screen, whereas the TL2 spectrometer line contains a parabolic screen, as presented in table I. The choice of radiators follows from extensive studies at CTF3 on how to mitigate the *vignetting* effect [16]. In this case vignetting means that less light is collected from the edges of the screen than from the center. It appears because the optical acceptance of the imaging system is limited and because OTR emission has a well-defined angular distribution [19]. Vignetting reveals itself as a non-uniform response and distorts the measured profile.

The screen response has been measured by looking at the amount of light collected by the CCD as the beam moves across the screen. Figure 7 presents the result of this study. For the diffusive screen, the vignetting effect is small over a range of ±30 mm, while the intensity from the parabolic screen is clearly position dependent. The position dependence is believed to come from a remnant vignetting effect while the off-center position of the masimum intensity comes from a misalignment [14]. This screen will be exchanged with a diffusive screen in January 2012.

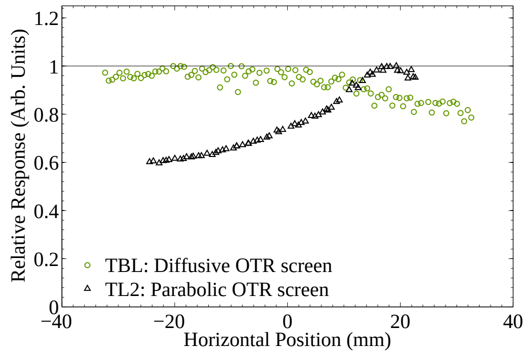

FIG. 7. Relative response of the OTR screens installed in the spectrometer lines. For the parabolic screen, the position dependence comes from vignetting. The offset of the maximum response is believed to be due to a misalignment.

B. Segmented Dump

A segmented beam dump uses the same detection principle as a Faraday cup. The incoming particles penetrate a metallic block, generate electromagnetic showers and are finally completely stopped. Every absorbed charge is detected as a current flowing to ground through a 50 Ω resistance. The physics process is fast, which allows for a fast sampling of the device. A horizontal segmentation of the metallic block, combined with individual data acquisition from each segment, provide a horizontal beam profile, which is then converted to energy spread through equation 1.

There are four segmented beam dumps installed at the CTF3 facility, and the experience from early models was the basis for the design of the segmented dump for TBL, see [18]. Special attention was paid to the known limitations to the system, such as sensitivity to misalignment and a non-uniform segment response. The more demanding beam characteristics at the location of the measurements was another main aspect.

1. Design and implementation

The design of the segmented dump was based on extensive FLUKA simulations [20, 21] using the Flair interface [22]. From these simulations, materials and dimensions of the detector system were chosen so that a good lifetime can be ensured and at the same time optimizing the resolution. See [18] for details regarding the design.

As previous segmented dumps, pure tungsten was chosen for the segments. With a high melting point it can withstand rather extreme thermal loads. Furthermore, tungsten is a dense material with a high stopping power. This means that the dimensions of the segments needed to stop the incoming particles is reduced compared to other materials, thus increasing the resolution. The segmented dump, installed in TBL in January 2011, has 32 segments 3 mm wide and spaced by 1 mm. Figure 8(a) shows a photograph of the segment assembly at the top left.

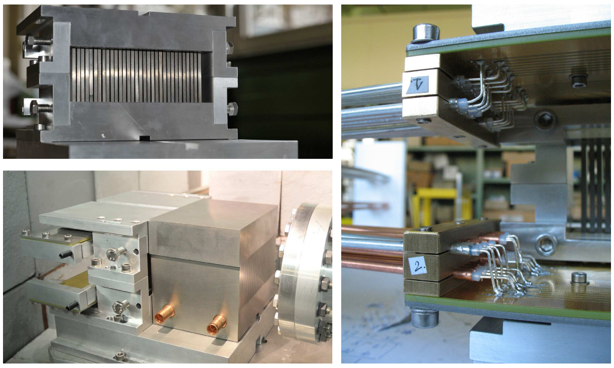

(a) Segment assembly (above) and complete system installed in the TBL beam dump (below).

(b) PCB and cable assembly seen from the back

FIG. 8. Photographs of the segmented dump assembly for TBL.

A water-cooled, multi-slit collimator is used as a thermal buffer for the segmented dump. The 100 mm long collimator absorbs most of the beam power and lets only a small fraction of the incoming particles pass through 400 μm wide slits, one in front of each segment. It is made of Inermet [23], a metallic compound with a high tungsten content, in order to keep it compact. Inermet was chosen over pure tungsten due to its machining properties, seeing that the tolerance requirements are strict for this application. The total energy absorbed by the collimator for every beam pulse was estimated from FLUKA simulations to be 500 J. This would lead to a local temperature increase of up to 90°C per beam pulse. With water-cooling the maximum temperature can be kept safely below 1000°C even for 5 Hz pulse frequency. Water-cooling also reduces the risk of thermal deformation from the beam impact, which is important considering the narrow slits. The slits, and the segments placed just after, are concentric with the bending center in order to match the angles of the incoming particles.

The detector system is placed outside of vacuum but integrated inside a beam dump, as shown in the lower picture in Fig. 8(a). Radiation hardness of all components are therefore important, as well as reliability once installed. For this reason, alumina was chosen as insulating material between and around segments [24], and semi-rigid, low-loss cables are used close to the signal source.

The beam-induced signal is acquired from each segment via a PCB connected to the segments through contact pins with a spring load. The semi-rigid cables, rated up to 18 GHz are soldered directly to the PCB, see Fig. 8(b), and then connected to long, standard, coaxial cables. The long cables constitute the second most important limitation to the time resolution of the system. The first limitation currently comes from the 250 MS/s sampling rate of the ADCs (type SIS 3320). With an operating range of ±2 V, these ADC cards call for 10−20dB attenuation of the signal amplitude. The attenuators are placed just before the ADCs.

2. *Estimated performance*

There are effects that are expected to broaden the measured beam profile. One is the presence of thin foils in the spectrometer line, such as the 50 μm aluminum screen for OTR generation, and 50 μm carbon foil, as described in section II. Additionally, there is a 100 μm aluminum vacuum window just upstream from the detector system. Together, these foils are expected to increase the beam divergence by 3 mrad, equivalent to a minimum beam width of $\sigma_{scatt} = 1.71$ mm at the position of the dump, as shown in Fig. 9.

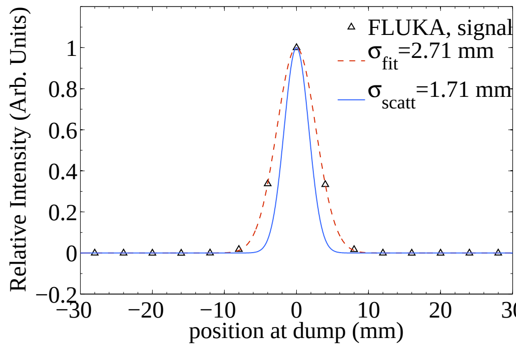

FIG. 9. FLUKA simulations: The distribution at the segmented dump of a 150 MeV beam, initially with a point-like cross section, after passing through thin elements in the spectrometer line (blue) and the relative signal per segment from a beam impinging on the middle segment (black, Gauss fit in dashed red). Both effects pose unavoidable resolution limitations to the system.

The segment width and spacing were optimized for containing both primary and secondary particles within the segment. Nonetheless, there will always be a certain level of crosstalk because of scattered particles. The effect of this crosstalk on the detector resolution has been investigated in FLUKA. By letting a 150 MeV electron beam impinge on the middle segment and study the signal leakage in form of scattered particles the lower resolution limit can be obtained. Figure 9 shows the result of this simulation: the relative signal from each segment as a function of horizontal position. The minimum beam width reproduced is thus $\sigma_{ref} = 2.71$ mm.

Considering these two main effects that will smear the beam profile before reconstruction, a lower resolution limit σ_{res} can be obtained by adding the corresponding beam widths in quadrature in the following manner:

$$\sigma_{res} \geq \sqrt{\sigma_{part}^2 + \sigma_{scatt}^2} = 3.2 \text{ mm} \implies \sigma_p \geq 0.9\% \quad (2)$$

A more extensive investigation of the effect of particle crosstalk on measured beam size is presented in Fig. 10. Beams of various widths have been used as input to FLUKA simulations. The width of the profile obtained from the segmented dump after beam absorption has been calculated and is here shown as a function of the true beam size. Once the 1σ beam width is >7 mm the overestimation from the segmented dump is less than 10%. The result of these simulations can be used to correct the measurement profile widths. Also, the broadening from scattering in foils can be estimated with FLUKA simulations for different beam energies and also used as an adjustment to the measurement.

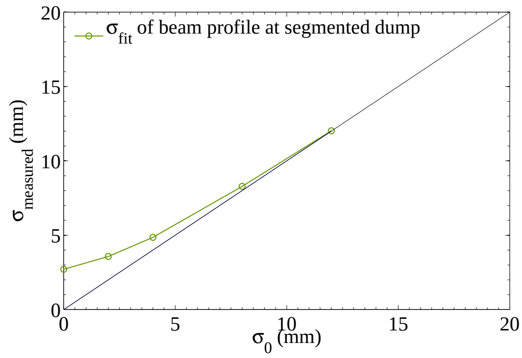

FIG. 10. FLUKA simulations: width of reconstructed distribution as a function of the width of the input beam.

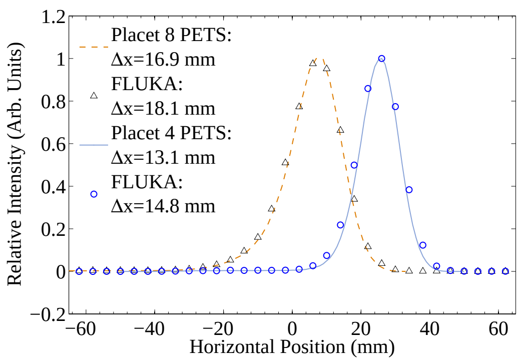

FIG. 11. FLUKA simulations of the detector performance on profile reconstruction. Expected beam distributions at the position of the segmented dump for 4 and 8 PETS, obtained with Placet, has been used as input.

The expected accuracy of the measurement was investigated with FLUKA. The final detector geometry was used, together with beam distributions obtained with Placet. As is shown in Fig. 11, the segmented dump reproduces the asymmetric beam profile well. For 4 PETS the beam size (FWHM) obtained with FLUKA is 13% larger than the reference beam profile. For 8 PETS, the equivalent value is 7%, and reaches 4% for 16 PETS. In all cases this overestimation is reduced to below 2% by subtracting in quadrature the broadening expected from segment crosstalk.

3. *Beam-based performance studies*

The performance of the segmented dump has been tested through a series of measurements. The response of individual segments and the alignment of the system has been tested using a dipole scanning technique, in which the beam is steered across the detector in small steps. Figure 12 shows the result of such a measurement. During a dipole scan each segment is used separately to scan through the beam. The resulting spectra are integrated over a selected time window, thus providing a beam profile as a function of dipole current - one profile for every segment. The peak of this profile is used as the segment response.

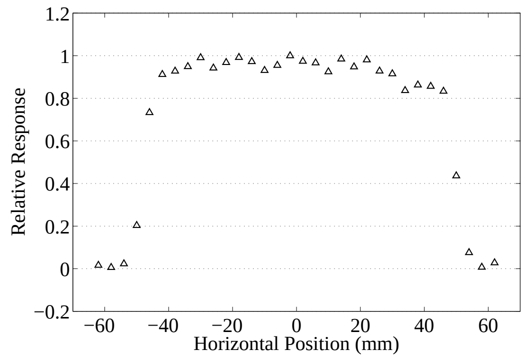

FIG. 12. Response of individual segments. The response is calculated by using each segment to scan the beam, then taking the maximum of the integrated profile.

The segmented dump in TBL gives a fairly uniform response. The steep intensity drop at ± 50 mm on both sides is explained by an aperture restriction from the 100 mm vacuum chamber. It is foreseen to remove this restriction in 2012. Small additional response variations from segment to segment are believed to arise from slit width variations and from minor misalignments of the segment with respect to the slit.

A scan measurement, using the middle segment, can offer not only a better granularity but also another way of studying the alignment of the device. Figure 13 includes both a single-shot measurement projected in time and the equivalent projection from such a scan, displaying an excellent agreement.

The OTR screen is used for cross-calibration of the device. The intrinsic beam size has been subtracted from

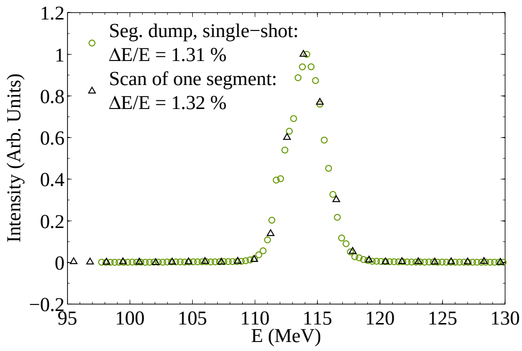

FIG. 13. A single-shot measurement compared to a scan measurement using the middle segment.

both measurements and the segmented dump profile has been corrected for particle crosstalk and scattering in foils. Figure 14 shows a single-shot measurement from the segmented dump and the OTR screen. In cases of large energy spreads, like the one presented, the agreement stays within the shot-to-shot accuracy of each measurement. At small energy spreads the segmented dump measures a 4% larger energy spread, as in Fig. 15, due to its limited granularity and resolution. For small energy spreads, the intrinsic beam size remains a more significant fraction of the measured beam size. The uncertainty of the measurement is thereby larger in this case. Assuming that the correct momentum spread measured by the OTR screen is correct, it can be concluded that the resolution of the segmented dump is 1%. This corresponds well to the value expected from simulations, refer to the discussion above in section III B 1.

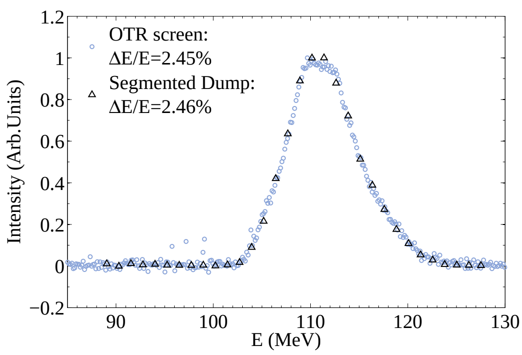

FIG. 14. Cross-calibration of the segmented dump with the OTR screen. The agreement between the OTR screen and the segmented dump is within the statistical fluctuations of the beam.

C. Single-slit Dump

The single-slit dump is installed in a 22.5° spectrometer line just upstream from TBL, marked as TL2 in the layout in Fig. 1 and in table I. The principle behind it is the same as that of a segmented dump. As the name suggests, it consists of a single detecting segment behind a collimator with a single slit. A drawing of the slit dump is presented in Fig. 16.

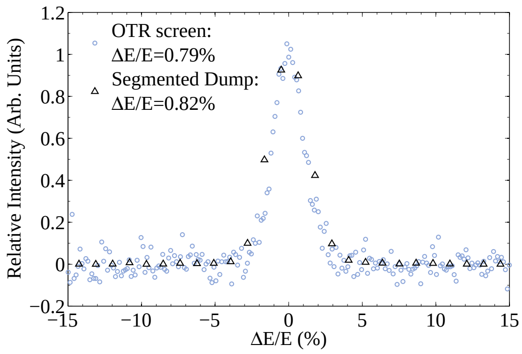

FIG. 15. Cross-calibration of the segmented dump with the OTR screen. Here, the energy spread is small compared to the resolution of the segmented dump. After applying corrections to the measurement, the segmented dump measurement gives a 4% overestimation compared to the OTR screen.

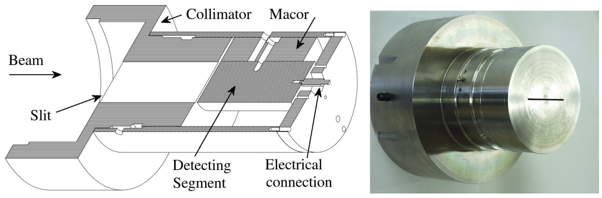

(a)Slit dump in cross section (b)Single-slit collimator

FIG. 16. The single-slit dump installed in the TL2 spectrometer line.

By adjusting the spectrometer magnet current, the slit dump can scan the beam and thus provide a multi-shot measurement of the time resolved energy profile. Evidently, a certain stability of the incoming beam will have to be assumed. It allows for a reference measurement of the energy profile before any deceleration has taken place.

The segment is a 100 mm long steel cylinder with a 50 mm radius. It is connected to a cable via a BNC connector and is kept electrically insulated by a 25 mm macor layer inside a steel support. The single-slit collimator consists of a 100 mm long steel cylinder with a 100 mm radius and a 1 mm wide slit. A surrounding support allows it to be directly attached to the vacuum chamber in the spectrometer line. An approximately 50 m long cable brings the signal to an electronics gallery where the signal is attenuated, $10-30$dB depending on the beam current, and then sampled at 100 MS/s by a SIS3300 ADC card, similarly to the segmented beam dump.

The spatial resolution is determined by the slit width, in this case 1 mm which corresponds to an energy spread of 0.12%. The time resolution of the slit dump is currently limited by the acquisition electronics in general and of the ADC in particular. If properly impedance matched, the device can reach a temporal resolution of 100 ps, thus requiring a much faster acquisition channel [25].

IV. MEASUREMENT EXAMPLES

During TBL operation the beam is monitored in several ways: BPMs for beam current and position, and OTR screens for beam size measurements. Figure 17 presents an example where a quadrupole scan and consecutive beam size measurements have been used to determine the Twiss parameters in TBL. The result is used for beam-size adjustment in spectrometry measurements (Eq. 1) by propagating the beam parameters through the lattice to the locations of the detectors. By focusing the beam on the detectors in the spectrometer line the influence of the intrinsic beam size is minimized and the resolution of the energy measurement is optimized.

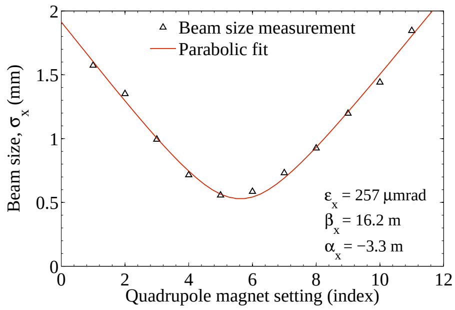

FIG. 17. An example of a quadrupole scan measurement in TBL. The beam width has been measured using the OTR screen for transverse profile at the end of TBL.

Figure 18 shows a typical beam energy spectrum as measured with the single-slit dump in TL2. The corresponding energy spectrum in TBL, as measured with the segmented dump, is presented in Fig. 19. The evolution over time of the beam energy can be extracted and compared with the equivalent for the incoming beam. In this way the deceleration is measured. The mean energy spread has been adjusted by the intrinsic beam size in respective locations. The segmented dump measurement has also been corrected for other known profile broadening effects, i.e. multiple scattering in foils and particle crosstalk between segments.

In Fig. 20 the measurement with the segmented dump is compared with the beam energy predicted from beam current and measurement of the RF power extracted from the PETS, from the same beam pulse. In this case, the measurement indicates similar fluctuations as those seen in the RF signals. The deceleration is expected to increase linearly with the beam current, which is confirmed by changing the current of the incoming beam. Figure 21 shows the average deceleration measured at beam currents 3 A, 6 A, 9 A and 12 A. The predicted deceleration is presented together with the measured and coincides with the linear fit to the measured values.

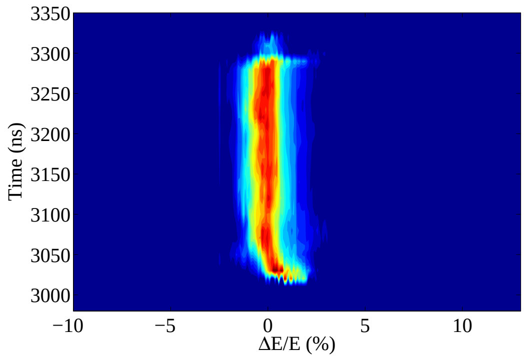

FIG. 18. Typical beam energy spectrum before entering TBL and the PETS for deceleration. The measurement is obtained with a single-slit dump using a dipole scanning technique. $E_0 = 117.9$ MeV, $I_{beam} = 13.5$ A, $\sigma_E = 0.83\%$.

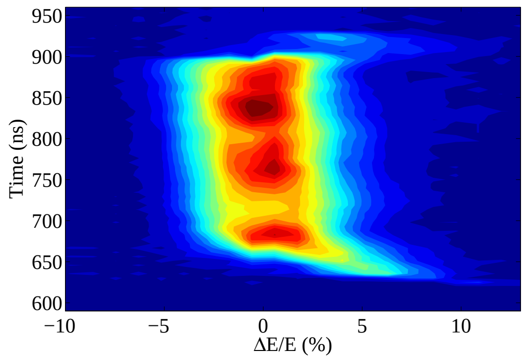

FIG. 19. Beam energy spectrum after deceleration in 4 PETS in TBL. $E_0 = 111.6$ MeV, $I_{beam} = 12$ A, $\Delta E/E_0 = 2.50\%$.

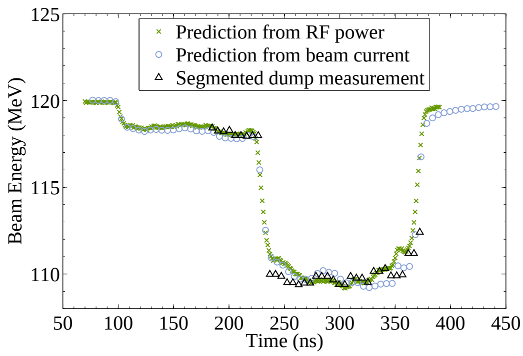

FIG. 20. The measured energy along the pulse showing the prediction from RF (4 PETS) and current measurements for comparison. Incoming beam: $I_{beam} = 18$ A, $E = 119$ MeV.

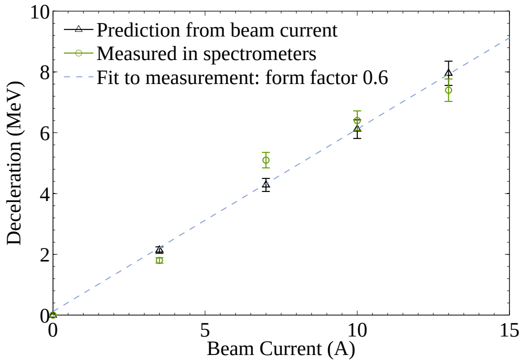

FIG. 21. The measured deceleration from 4 PETS as a function of beam current. The deceleration expected from beam current measurements are shown for comparison.

V. CONCLUSION

The Test Beam Line at CTF3 is under commissioning and 9 out of the total 16 Power Extraction and Transfer Structures have been installed. At the nominal beam current of 28 A a 5.2 MeV deceleration is expected from each PETS. The extracted power is measured and compared with the measured energy loss of the beam.

Two diagnostic sectors are employed for monitoring the beam in TBL: one before and one after the deceleration. Each sector contains an OTR screen system for transverse profiling, another OTR screen for high resolution, average energy and energy spread measurements, and a third device for time-resolved spectrometry.

A segmented beam dump has been designed especially for time-resolved spectrometry in TBL. It provides single-shot measurement with a temporal resolution of 5 ns and can monitor energy spreads down to 1%. Beam-based cross-calibration shows that the segmented beam dump agrees well with the spectrometer OTR screen.

Preliminary results from the TBL commissioning shows that the deceleration predicted from RF power and beam current measurement agrees well with what has been measured in the spectrometer lines. Fluctuations along the pulse in the RF signals are also recognized in the segmented dump measurement. A continuation of the beam measurements will be necessary for a full characterization of the deceleration process. The measurements will be compared with simulations for a deeper understanding of the beam. Eventually, the study will be completed with a higher beam current and a higher number of PETS.

ACKNOWLEDGMENTS

Thanks to the CTF3 collaboration for support and construction of TBL. We wish to acknowledge the support of the CTF3 operation team for its everyday help and support during TBL operation. Author M. Olvegård is supported by the EU under contract PITN-GA-2008-215080.

[1] H. Braun *et al.*, CERN Report No. CLIC-Note-764, 2008.
[2] E. Adli *et al.*, Phys. Rev. ST Accel. Beams 14, 081001 (2001)
[3] G. Geschonke and A. Ghigo *et al.* (The CLIC Study Team), CTF3 Design Report No. CERN/PS-2002-008 (RF), 2002.
[4] S. Döbert *et al.*, in *Proceedings of the 25th International Linear Accelerator Conference, Tsukuba, Japan, 2010*, p. 85.
[5] R. Corsini *et al.*, in *Proceedings of the 9th European Particle Accelerator Conference, Lucerne, Switzerland, 2004*, p. 39
[6] W. Farabolini *et al.*, in *Proceedings of the 2nd International Particle Accelerator Conference, San Sebastian, Spain, 2011*, p. 29.
[7] E. Adli, Ph.D. thesis, University of Oslo, 2009.
[8] F. Toral *et al.*, in *Proceedings of the 11th European Particle Accelerator Conference, Genoa, Italy, 2008*, p. 1517.
[9] I. Syratchev, D. Schulte and E. Adli, in *Proceedings of the 22nd Particle Accelerator Conference, Albuquerque, USA, 2007*, (IEEE, New York, 2007), p. 2194
[10] D. Schulte *et al.*, CERN Report No. CERN-PS-2000-028-AE, 2000.
[11] "The tracking code PLACET", `https://savannah.cern.ch/projects/placet/`, 2010.
[12] T. Lefèvre *et al.*, in *Proceedings of the 10th European Particle Accelerator Conference, Edinburgh, United Kingdom, 2006*, p. 1205.
[13] J. J. García-Garrigós *et al.*, in *Proceedings of the 10th European Workshop on Beam Diagnostics and Instrumentation for Particle Accelerators, Hamburg, Germany, 2011*, p. 335
[14] M. Olvegård *et al.*, in *Proceedings of the 10th European Workshop on Beam Diagnostics and Instrumentation for Particle Accelerators, Hamburg, Germany, 2011*, p. 413
[15] E. Bravin, T. Lefèvre and C. Vermare, CERN AB BDI Report No. 050, 2003.
[16] C. P. Welsch, E. Bravin and T. Lefèvre, Rev. Adv. Mater. Sci 16 (2007), p. 73.
[17] B. Bolzon *et al.*, in Proceedings of the DITANET International Conference: Accelerator Instrumentation and Beam Diagnostics, Seville, Spain, 2011.
[18] M. Olvegård *et al.*, in *Proceedings of the 1st International Particle Accelerator Conference, Kyoto, Japan, 2010*, p. 1113.
[19] L. Wartski, Ph.D. thesis, Universitè de Paris-Sud, 1976.
[20] G. Battistoni *et al.*, in *Proceedings of the Hadronic Shower Simulation Workshop, Batavia, U.S.A, 2006* (AIP Conference Proceeding 896, 2007), p. 31.
[21] A. Fasso *et al.*, CERN Report No. CERN-2005-10; INFN Report No. INFN/TC_05/11; SLAC Report No. SLAC-R-773, 2005.

[22] V. Vlachoudis, in *Proceedings of the International Conference on Mathematics, Computational Methods and Reactor Physics (M&C 2009), Saratoga Springs, U.S.A., 2009*.

[23] "Densimet® and Inermet® Tungsten Alloys", http://www.plansee.com/lib/SD-DI-02.pdf, 2010.

[24] P. Beynel *et al.*, CERN Report No. CERN-1982-10, 1982.

[25] D. Egger *et al.*, in *Proceedings of the 10th European Workshop on Beam Diagnostics and Instrumentation for Particle Accelerators, Hamburg, Germany, 2011*, p. 431.